Anisotropy of magnetic susceptibility (AMS) analysis of the Gonjo Basin as an independent constraint to date Tibetan shortening pulses

Shihu Li[1, 2*], Douwe J.J. van Hinsbergen[3], Zhongshan Shen[1,4,5], Yani Najman[2], Chenglong Deng[1,4,5], Rixiang Zhu[1,4,5]

1 State Key Laboratory of Lithospheric Evolution, Institute of Geology and Geophysics, Chinese Academy of Sciences, Beijing 100029, China

2 Lancaster Environment Centre, Lancaster University, LA1 4YQ, Lancaster, UK

3 Department of Earth Sciences, Utrecht University, Utrecht, The Netherlands

4 Institutions of Earth Science, Chinese Academy of Sciences, Beijing 100029, China

5 College of Earth and Planetary Sciences, University of Chinese Academy of Sciences, Beijing 100049, China

[*]Corresponding author (S. Li: s.li31@lancaster.ac.uk)

Abstract The Tibetan Plateau accommodated major upper crustal shortening during Indian Plate oceanic and continental lithosphere subduction. Deciphering whether shortening was continuous or episodic, and how it correlates to major geodynamic changes, is challenging. Here we apply anisotropy of magnetic susceptibility (AMS), a sensitive syn-sedimentary strain indicator, to a ~3 km thick magnetostratigraphically dated sedimentary section (69–41.5) in eastern Tibet. AMS shows weak oblate fabrics from 69-52 Ma, followed by a sudden change to prolate fabrics with increasing anisotropy degree at ~52 Ma, dating a sudden increased syn-sedimentary shortening strain. This change coincides with enhanced sedimentation rates and syn-sedimentary vertical-axis rotations of the Gonjo Basin, and suggests a causal link to a marked India-Asia convergence rate deceleration. We show that AMS analysis provides a strong tool to distinguish between climatic and tectonic causes of sedimentological change, and is an asset in identifying discrete tectonic pulses in intensely deformed terrane.

Plain Language Summary How the Tibetan Plateau evolved during India-Asia convergence and collision is notoriously challenging to decipher. Use of sedimentary records to date periods of tectonic activity is a popular approach, yet deconvolving tectonic versus climate signals can be challenging**.** The anisotropy of magnetic susceptibility (AMS) is an effective and sensitive technique that reveals tectonic stress fields during sedimentation, and changes therein, even in weakly deformed clastic sedimentary rocks. We report a detailed record of AMS data from a ~3 km thick section of redbeds from the Gonjo Basin of eastern Tibet. Previous magnetostratigraphy dated deposition from 69 to 41.5 Ma, during which time marked sedimentation rate increases and simultaneous vertical-axis rotations were interpreted to reflect shortening pulses. Our new data indicate an increased shortening strain at ~52 Ma, demonstrating that the sedimentation rate changes are tectonic rather than climatic in origin,

showing that a pulse in crustal shortening of Tibetan occurred simultaneous with a marked ~52 Ma onset of deceleration of India-Asia convergence. We show that applying a suite of paleomagnetic and rock magnetic techniques, including magnetostratigraphy and sedimentation rate calculation, vertical axis rotation, and AMS analysis provides a strong tool to differentiate tectonic versus climatic influence on a sediment archive, allowing to sharply date discrete deformation phases in intensely deformed regions that evolved over long periods of time.

Key Points:

1. The AMS of the Gonjo Basin records sedimentary fabrics overprinted by weak shortening;
2. The AMS of the Gonjo Basin indicates an increased strain related to shortening at ~52 Ma;
3. AMS with precise age constraint provides a strong tool to date deformation phases, allowing to discriminate between tectonic vs climatic influences on sediments

1. Introduction

The Tibetan Plateau has undergone a long history of shortening at least since the Cretaceous (e.g., Kapp and DeCelles, 2019). Identifying its deformation history is of importance for analysis of geodynamics as well as paleoclimate. During the Plateau's long deformation history, several sharp geodynamic and climatic events occurred that are thought to be reflected in, or even caused by Tibetan shortening. For instance, the India-Asia convergence rate has undergone major changes around e.g., 70, 52, and 20 Ma (Molnar & Stock, 2009; van Hinsbergen et al., 2011) and the reflection of these events in the deformation of the upper crustal in Tibet may provide novel constraints on the underlying dynamic drivers (e.g. Li et al., 2020). Meanwhile, there are marked changes in regional climate, such as aridification, that may at least in part relate to deformation and/or uplift events of Tibet (e.g., Guo et al. 2002). Establishing whether shortening in Tibet was gradual or pulsed, and if the latter, what the timing and distribution of such pulses may have been, will thus be helpful in advancing our understanding of the causes and consequences of Tibetan Plateau formation. Yet this is challenging; geological archives that hold clues to the Plateau's long-term deformation history are provided by sedimentary basins across the Tibetan Plateau, but variations in sedimentary infill may in principle be caused by climatic (e.g. Molnar, 2004) as well as tectonic influences, making such changes difficult to interpret.

Recently, a high-resolution magnetostratigraphic study (Li et al., 2020) on a ~3 km thick stratigraphy of the Gonjo Basin, located in east-central Tibet (Fig. 1a), revealed a 69–41.5 Ma age range for the basin. The age model suggested that the Gonjo Basin experienced two short periods of rapid sedimentation (~20 cm/yr) at 69–64 Ma and 52–48 Ma, within longer-term periods of low sedimentation (7–8 cm/yr) at 64–52 Ma and 48–41 Ma (Fig. 2h). Because paleomagnetic declinations showed that the Gonjo Basin experienced vertical axis rotations during these high sedimentation rate intervals but not during the low sedimentation rate intervals, the high sedimentation rate intervals were interpreted to reflect periods of enhanced tectonic deformation, which was further interpreted as crustal shortening pulses given the contractional setting in eastern Tibet (Li et al., 2020). This is interesting because the first pulse of deformation since 69 Ma is roughly synchronous with a rapid acceleration of India-Asia convergence rate, while the second pulse of deformation since 52 Ma is synchronous with a major deceleration of India-Asia convergence rate. These interpretations predict that the periods of high sedimentation rate coincide with enhanced shortening strain, which should then be recorded in the sedimentary record.

In this paper, we study the Gonjo section in detail using anisotropy of magnetic susceptibility (AMS). This is a petrofabric tool able to determine the preferred orientation of particles under an external field (e.g., gravity, wind, magnetic field, flow and strain) during deposition and diagenesis of rocks and is locked in after sediment consolidation. The AMS method has been widely employed as an easy, fast, economic, and sensitive rock strain indicator, and has been widely successfully applied (Gilder et al., 2001; Gong et al., 2009; Li et al., 2014; Maffione et al., 2015; Parés et al., 1999; Soto et al., 2009; Tang et al., 2012; van Hinsbergen et al., 2005). We here apply the AMS as an independent method to constrain the timing of crustal shortening pulses, and to test whether the high sedimentation rate intervals coincide with enhanced AMS fabrics.

2. Geological setting and methods

The Gonjo Basin (30.85°N, 98.3°E) is located in the eastern part of the Qiangtang terrane, northeast of the Eastern Himalayan Syntaxis (Fig. 1a). The subsidence and structure of the Gonjo Basin was controlled by the Yangla thrust fault to the east, which carried Triassic rocks over the basin margin in the northeast (Studnicki-Gizbert et al., 2008; Tang et al., 2017; Fig. 1b). The basin sediments are now exposed in an asymmetric syncline (Fig. 1c), where the thickness of strata in the western limb is significantly thicker and shallower than that in the eastern limb. This, together with the presence of growth strata in the eastern part of the basin, has led to the interpretation that the Gonjo Basin was a syn-contractional basin (Studnicki-Gizbert et al., 2008). Basin structures, sedimentation facies, and varied paleocurrent directions suggested that the Gonjo Basin was fed by proximal source (Studnicki-Gizbert et al., 2008; Tang et al., 2017). The strata in the Gonjo Basin are dominated by red-colored mudstones, sandstones, and rare conglomerates with a thickness of >3000 m (Xizang BGMR, 1982).

A total of 542 samples along the 3325 m magnetostratigraphic section were measured for AMS, using a KLY-3 Kappa bridge (AGICO) with an automated sample handling system and an applied field of 300 A/m at a frequency of 875 Hz. Each sample was rotated through three orthogonal planes. The AMS parameters, including $K_{1/2/3}$ (maximum/intermediate/minimum of the principle axes), Km (mean susceptibility), P_J (corrected degree of anisotropy), and T (shape factor) were calculated following the definitions in Tarling and Hrouda (1993). Generally, Km reflects the concentration of magnetic minerals, P_J quantifies the degree of anisotropy, and T reflects the shape of the susceptibility ellipsoid. $0<T\leq1$ indicates oblate shapes, whereas $-1\leq T<0$ indicates prolate shapes, and $T = 0$ corresponds to neutral shapes (Jelinek, 1981).

Previous rock magnetic studies (Li et al., 2020; Tong et al, 2017; Zhang et al., 2018) have confirmed that hematite is the dominant magnetic mineral in the sedimentary rocks of the Gonjo Basin, with minor contribution of magnetite in some samples. To further identify the relative content of magnetite and hematite in the sediments, the high field isothermal remanent magnetization (IRM) acquisition curves were analyzed based on cumulative log Gaussian analysis (Kruiver et al., 2001).

3. Results

Figure 1d shows stereonet projections of the three principle axes for all the samples before and after bedding correction. In *tilt-corrected* coordinates, the K_1 directions are generally subhorizontal and well grouped in NNW-SSE direction, and generally parallel to the fold axis that deformed the basin fill; the K_3 axes are near bedding perpendicular and show a slight girdle distribution toward SW. Such distributions of the principal anisotropy axes are inconsistent with the varied paleocurrent directions of the Gonjo Basin, but instead are commonly found in folded sediments in foreland basin (Charreau et al., 2009; Gilder et al., 2001; Huang et al., 2005; Kodama, 1997; Li et al., 2014; Tang et al., 2012), indicating that the original sedimentary fabric was overprinted by weak tectonic-induced strain. Interestingly, the AMS fabrics and parameters show significant changes with stratigraphic position in the section (Figs. 2 and 3), and are subdivided into three intervals:

Interval I (0-765 m, 69-65.4 Ma) is characterized by the largest values of P_J (ranging from 1.01-1.44, average: 1.13) and the mean magnetic susceptibility Km (ranging from 18-488 x 10^{-6} SI, average:188 x 10^{-6} SI) except the lowest 80 m (Figs. 2b-2c). The K_1 axes are distributed in NNW-SSE directions and K_3 inclinations are almost perpendicular to the bedding plane (average: 87.6º, see Supplementary Table S1 for the statistical mean direction of principle axes and AMS parameters) (Fig. 3a). The AMS ellipsoid shapes defined by K_1, K_2, and K_3 are dominantly oblate with T typically >0.5 (average value: 0.6) (Fig. 2d).

Interval II (765-2154.5 m, 65.4-52 Ma) is marked by a sharp decrease of P_J (from 1.005-1.1, average: 1.03) and Km (from 32-287 x 10^{-6} SI, average: 115 x 10^{-6} SI), which subsequently show a gradual increase upward (Figs. 2b-2c). The K_1 axes are distributed subhorizontally in ~N-S orientation and K_3 axes are mostly perpendicular to the bedding plane (average: 80.5º) (Fig. 3b). However, at the lower part of this interval, the K_3 orientations are shallowed and the AMS axes are scattered (Figs. 2e-2f and 3b). We suspect that this is due to the low susceptibility in these intervals, which prohibits a precise AMS direction to be measured. Despite change of magnetic susceptibility, the shape parameter T oscillates uniformly around T = 0 (the threshold value of prolate to oblate) with an average value of 0.1 in this interval (Fig. 2d), suggesting a dominance of neutral shapes in interval II.

Like interval II, P_J and Km in interval III (2154.5-3325 m, 52-41.5 Ma) also increase upward in the strata (Figs. 2b-2c). P_J ranges from 1.007-1.09 with an average value of 1.04, and Km varies from 69-297 x 10^{-6} SI with an average value of 173 x 10^{-6} SI. The most prominent feature in interval III is the change of T to negative values (mean value: -0.24) (Fig. 2d), which indicates prolate shapes of the AMS ellipsoid in this interval. This is consistent with the distribution of K_3 orientations (average: 59.5º) describing a SW–NE girdle distribution (Fig. 3c), suggesting that K_3 and K_2 are almost equal, or, in other words, the minimum axis parallel to the shortening direction becomes near-equal to the compaction-induced, vertical shortening (Fig. 2c). Notably, the grouping of K_1 axes in interval III is significantly tighter than in intervals I and II (Fig. 3c).

The IRM component analyses identified two components in all the samples (Fig. 4): a minor low-coercivity component and a pronounced high-coercivity component. For the low-coercivity component, most samples have $B_{1/2}$ (the field at which half of the saturation IRM is reached) larger than 100 mT, which could be maghemite or fine-grained hematite. The two samples from interval I have $B_{1/2}$ less than 50 mT, which is a reasonable value for magnetite. The high-coercivity component of all samples has $B_{1/2}$ between ~350–900 mT, which is consistent with the magnetic properties of hematite.

4. Discussion

4.1 Source of the magnetic susceptibility

Magnetic susceptibility of rocks contains contributions of diamagnetic, paramagnetic matrix minerals, ferrimagnetic and antiferromagnetic minerals. AMS residing in magnetite reflects a preferred grain shape orientation, whereas AMS due to hematite or paramagnetic minerals reflects preferred crystallographic orientation (Borradaile and Henry, 1997; Parés et al., 1999), which is controlled by tectonic strain. Therefore, it is essential to identify which mineral(s) dominate(s) the AMS when applying AMS data to tectonics. As the volume susceptibility of magnetite (~1 SI, Tauxe, 2010) is ~1000 times greater than most minerals (Gilder et al., 2001; Parés et al., 2004), magnetite will dominate the magnetic behavior of sediments if magnetite content exceeds 0.5% of the iron oxide. The mean magnetic susceptibility (Km) of Gonjo sediments, however, varies from 18-488 x 10^{-6} SI with a mean value of 155 x 10^{-6} SI. The overall very weak values of bulk susceptibility argue against a significant contribution from magnetite and suggest that the susceptibility, and hence the AMS are dominated by antiferromagnetic (e.g., hematite) and paramagnetic minerals. This is consistent with our IRM component analysis results which suggests that hematite is the dominant magnetic mineral in the sedimentary sequence of the Gonjo Basin, with minor contribution from magnetite only at the bottom of the section (Fig. 4).

As shown in Fig. 1d, P_J exhibits a very weak correlation to the Km, suggesting that magnetic minerals concentration may partly control P_J. However, our results show that T is independent of Km, and both P_j and T are independent of lithology. Therefore, the AMS of the Gonjo Basin recorded a crystallographic preferred orientation of hematite and paramagnetic minerals aligned by tectonic strain. The clustering of K_3 inclinations to near vertical after bedding correction indicates that the magnetic fabrics were acquired before the tilting of the sedimentary sequences, i.e. during or shortly after deposition during incipient deformation and diagenesis and mainly related to layer-parallel shortening (Larrasoaña et al., 2004; Parés et al., 1999; 2004; Soto et al., 2009). This is further supported by the coincident change between AMS K_1 orientations and paleomagnetic declinations: both indicate a slight counterclockwise rotation at 69–67 Ma, no significant rotation from 67–52 Ma, a clockwise rotation at 52–48 Ma, followed by no significant rotation between 48–41.5 Ma (Figs. 2f-2g). This interesting result, as also observed in the Subei Basin of northeast Tibet (Gilder et al., 2001), suggests that the AMS results of the Gonjo Basin are robust recorders of tectonic strain and changes therein during the sedimentary deposition.

4.2 Relationship between AMS and strain

AMS can be geometrically described by an ellipsoid, which is qualitatively related to the finite strain state. Ramsay and Huber (1983) developed the classical relationship between strain magnitude and cleavage intensity in sediments, where the latter can be described by the magnetic fabric. Six main stages of fabric development have been distinguished with increasing strain: undeformed condition, earliest deformation, pencil structure, weak cleavage, strong cleavage, and stretching lineation (Parés et al., 2004). We will briefly describe the first four stages before obvious cleavage can be observed at outcrop scale.

An ‘undeformed condition’ of a sedimentary fabric is characterized by parallelism of the magnetic foliation and the bedding plane, with a relatively low degree of anisotropy and an oblate shape of the AMS ellipsoid. The K_1 and K_2 axes are disorderly scattered within a plane parallel to bedding, whereas the K_3 axes are vertical to the bedding plane. In case the sediments are transported by wind or water, a weak magnetic lineation may have formed by alignment of minerals which can be reflected by K_1 (e.g., Zhu et al., 2004), either parallel or normal to the wind/paleocurrent direction, depending on the hydrodynamic condition (Tauxe, 2010). After minor layer-parallel shortening, an ‘earliest deformation’ stage is formed, which is characterized by grouping of K_1 to develop magnetic lineation that is perpendicular to the shortening direction and parallel to the tensile direction. The magnetic foliation is still parallel to bedding plane and K_3 axes are normal to the magnetic foliation. As shortening increases, the clustering of K_1 and K_2 continues to increase, while K_3 will form a girdle with K_2 that is parallel to the principal strain axis, and the AMS ellipsoid changes from oblate to prolate to produce a 'pencil structure' fabric (e.g., Maffione et al., 2015; Parés et al., 1999). Further increasing strain leads to the production of a weak or incipient cleavage that crosscuts bedding, corresponding to a 'weak cleavage' fabric. The K_3 distribution gradually changes from girdle to cluster parallel to the bedding plane and the shortening direction, whereas the magnetic ellipsoid remains prolate.

4.3 A shortening pulse of Tibet at ~52 Ma

Our AMS results between 69 and 65.4 Ma display an oblate ellipsoid with K_3 normal to bedding plane, and K_1 subhorizontal and gathered around a NNW–SSE direction. This distribution is consistent with an original sedimentary fabric overprinted by a subtle NE–SW shortening, representing the earliest deformation stage. The AMS changes from oblate to neutral shape since 65.4 Ma associated with a significant decrease of P_J and Km. This is consistent with the synopsis P_J-T path of the development of magnetic anisotropy with increasing deformation intensity (Fig. 3). We interpret that the AMS between 65.4 and 52 Ma represents a transition between the earliest deformation and the pencil structure that appears in 52 Ma and younger sediments, where the AMS is characterized by prolate magnetic ellipsoids, and the K_1 are tightly clustered in a NNW–SSE, fold axis-parallel orientation, and the K_3 are distributed along a moderate girdle with K_2. This is consistent with the pencil structure stage, implying a significant increase in syn-sedimentary shortening strain, and therefore tectonic deformation during this interval. Moreover, our results suggest that P_J is more sensitive to magnetic content, whereas T is more related to strain change, and therefore T is a more reliable parameter to provide information regarding tectonic deformation.

The magnetostratigraphic age model for the Gonjo Basin (Fig. 2i, Li et al., 2020) showed that the sedimentation rate in the Gonjo Basin increased from ~8 cm/kyr to ~20 cm/kyr at ~52 Ma (Fig. 2h). Our AMS results positively test the prediction of Li et al. (2020) that the sedimentation rate increase coincides with a sudden increase in tectonic shortening strain at 52 Ma, and therefore reflects a tectonic origin.

Tectonic deformation of the Tibetan Plateau at ~52 Ma has been identified in previous studies. In north and northeast Tibet, a series of Cenozoic sedimentary basins were developed as a result of this deformation, e.g., Qaidam, Xining, and Lanzhou basins (Fig. 1a). The Cenozoic strata unconformably overlie pre-Cenozoic strata, and are dominated by conglomerates and coarse sandstones at the base. The initial age of these basins has been magnetostratigraphically constrained at ~52-54 Ma (Dai et al., 2006; Fang et al., 2019; Ji et al., 2017; Yue et al., 2001). In the central part of Tibet, a magnetostratigraphic study of Hoh Xil Basin indicates a rapid increase of sedimentation rate at ~54 Ma (Jin et al., 2018). Low-temperature thermochronology studies indicate that the Altyn Tagh and the southern Qilian Shan-Nan Shan faults initiated at ~50 Ma (Cheng et al., 2015; Jolivet et al., 2001; Yin et al., 2002;), the West Qinling fault began thrusting at ~50 Ma (Clark et al., 2010), and southern and central Tibet experienced rapid exhumation around ~55-48 Ma (Hetzel et al., 2011; Jian et al., 2018; Staisch et al., 2014). Furthermore, paleomagnetic results indicate that northeast (Dupont-Nivet et al., 2004), east (Li et al., 2020) and southeast (Li et al., 2017) Tibet underwent clockwise rotation starting at ~50 Ma. These estimates rely on different types of datasets, each with their own uncertainty. The integrated high-resolution magnetostratigraphy of the Gonjo Basin providing detailed age control (Li et al. (2020) and now coupled with the extensive AMS analysis provided in this paper firmly confirms that much of these features result from a sudden increase in shortening strain starting at ~52 Ma.

4.4 Application of AMS to decipher long-term shortening history

The onset of India-Asia collision, although highly controversial, has been constrained at 59±1 Ma, when the first Asian sediments arrived in the Tethys Himalayan stratigraphy that marks the northernmost continental crust on the Indian plate (Hu et al., 2015). The AMS ellipsoid shape and parameters from the Gonjo Basin, however, do not reveal a significant change at this inferred time of collision (Figs. 2b-f), which is in line with the absence of a regional change in sedimentation rate and paleomagnetic declinations from the Gonjo Basin (Fig. 2; Li et al., 2020). Instead, significant upper crustal shortening of eastern Tibet at ~52 Ma as observed by our AMS coincide with the increase of sedimentation rates and clockwise rotation of the Gonjo Basin (Li et al., 2020), and the sudden drop of India-Asia convergence rate from ~160 mm/yr to ~80 mm/yr starting around 52 Ma (Copley et al., 2010; van Hinsbergen et al., 2011). All these lines of evidence suggest that, although the India-Asia initial collision began at 59±1 Ma, significant tectonic deformation in Tibet and slow-down of India did not occur until 52 Ma, a few million years later than the initial collision.

Given its setting, shortening of the Tibetan Plateau has long been interpreted as a direct result of collision of India with Asia (e.g., Patriat and Achache, 1984), and the mismatch between onset of collision and upper crustal shortening increase may be surprising. This may suggest that the sedimentary record in the Himalaya reflected either collision of a far-traveled Asia-derived arc remnant with the northern Indian margin, rather than with Asia (e.g., Kapp and DeCelles, 2019), or collision of an extended continental from India with Asia (van Hinsbergen et al., 2012). On the other hand, comparison with other modern orogens shows that there is no systematic relationship between upper crustal shortening and collision. For instance, the Andean orogen formed due to upper crustal shortening during oceanic subduction (e.g. Oncken et al., 2006), whereas long-lived continental subduction in the Mediterranean region has for 100 Myr or more been associated with widespread upper crustal extension instead of shortening (van Hinsbergen et al., 2020). It has long been shown that significant 'Andean-style' orogenesis occurred in Tibet well before initial collision with India (e.g., Kapp and DeCelles, 2019, and references therein). Our results may suggest that also the Cenozoic shortening, and by inference uplift of the Tibetan Plateau may not be directly tied to the nature of the lithosphere consumed at the south Tibetan plate boundary.

The slow-down of India at ~52Ma may reflect deeper-seated processes related to the interaction of the subducting Indian lithosphere with the mantle (van Hinsbergen et al., 2019; Zhu et al., 2015). However, regardless of the geodynamic causes underpinning the India-Asia plate motion changes or the 52 Ma shortening pulse in Tibet, the analysis of geodynamic causes of upper crustal deformation requires tight age constraints between collisional, plate kinematic, and climatic processes. Our analysis shows that integrated paleomagnetic and rock magnetic datasets can provide such tight age constraints that may lie at the basis for further analysis of the geodynamic and climatic processes that shape the Earth's crust and surface.

5. Conclusions

In this study, we present AMS results from the Gonjo Basin of 69-41.5 Ma, which provide information about the strain change and tectonic deformation of eastern Tibet during the India-Asia collision. The AMS results suggest that the Gonjo Basin was under ~NNE-SSW direction shortening persistently from 69-41.5 Ma, consistent with the previously interpreted syn-contractional nature of the basin. Our AMS results provide independent evidence that the increase of sedimentation rates of Gonjo Basin at 52 Ma as indicated by previous magnetostratigraphic analysis reflects a tectonic pulse and that there was no such pulse upon initial continental collision recorded in the Tibetan Himalaya at 59±1 Ma. From this we infer that upper crustal shortening may not directly reflect the change in nature of the subducting lithosphere, and can thus not be used to date collision. Our results illustrate that the deciphering of geodynamic, or climatic, influence on plateau formation and plateau rise and vice versa require independent, high-resolution dating of upper crustal shortening, and that integrated paleomagnetic research may provide such dating.

Acknowledgements This work was funded by the Strategic Priority Research Program of the Chinese Academy of Sciences (XDA13010106) and the National Natural Science Foundation (41888101, 41690112, and 41761144065). S.L. acknowledges the further support from the Royal Society-K.C.Wong International Fellowship at Lancaster University. D.J.J.v.H acknowledges NWO Vici grant 865.17.001. The original AMS data of this paper can be accessed through the public domain repository Zenodo at https://doi.org/10.5281/zenodo.3666760.

References

Borradaile, G., and B. Henry (1997), Tectonic applications of magnetic susceptibility and its anisotropy, *Earth-Sci. Rev.*, *42*(1), 49-93. Doi: 10.1016/S0012-8252(96)00044-X.

Charreau, J., Y. Chen, S. Gilder, L. Barrier, S. Dominguez, R. Augier, S. Sen, J. P. Avouac, A. Gallaud, F. Graveleau, Q. C.Wang (2009), Neogene uplift of the Tian Shan Mountains observed in the magnetic record of the Jingou River section (northwest China), *Tectonics*, *28*. Doi: 10.1029/2007tc002137.

Cheng, F., Z. Guo, H. S. Jenkins, S. Fu, and X. Cheng (2015), Initial rupture and displacement on the Altyn Tagh fault, northern Tibetan Plateau: Constraints based on residual Mesozoic to Cenozoic strata in the western Qaidam Basin, *Geos.*, *11*(3), 921-942. Doi: 10.1130/ges01070.1.

Clark, M. K., K. A. Farley, D. Zheng, Z. Wang, and A. R. Duvall (2010), Early Cenozoic faulting of the northern Tibetan Plateau margin from apatite (U–Th)/He ages, *Earth Planet. Sci. Lett.*, *296*(1), 78-88. Doi: 10.1016/j.epsl.2010.04.051

Copley, A., J. P. Avouac, and J. Y. Royer (2010), India-Asia collision and the Cenozoic slowdown of the Indian plate: Implications for the forces driving plate motions, *J. Geophys. Res.*, *115*(B03410). Doi: 10.1029/2009JB006634

Dai, S., X. M. Fang, G. Dupont-Nivet, C. H. Song, J. P. Gao, W. Krijgsman, C. Langereis, and W. L. Zhang (2006), Magnetostratigraphy of Cenozoic sediments from the Xining Basin: Tectonic implications for the northeastern Tibetan Plateau, *J. Geophys. Res.*, *111*(B11). Doi 10.1029/2005jb004187.

DeCelles, P. G., P. Kapp, G. E. Gehrels, and L. Ding (2014), Paleocene-Eocene foreland basin evolution in the Himalaya of southern Tibet and Nepal: Implications for the age of initial India-Asia collision, *Tectonics*, *33*(5), 2014TC003522. Doi: 10.1002/2014TC003522.

Ding, L., S. Maksatbek, F. Cai, H. Wang, P. Song, W. Ji, Q. Xu, L. Zhang, Q. Muhammad, and B. Upendra (2017), Processes of initial collision and suturing between India and Asia, *Sci. China Earth Sci.*, *60*(4), 635-651. Doi: 10.1007/s11430-016-5244-x.

Dupont-Nivet, G., B. K. Horton, R. F. Butler, J. Wang, J. Zhou, and G. L. Waanders (2004), Paleogene clockwise tectonic rotation of the Xining-Lanzhou region, northeastern Tibetan Plateau, *J. Geophys. Res.*, *109*(B04401). Doi: 10.1029/2003jb002620.

Fang, X., et al. (2019), Cenozoic magnetostratigraphy of the Xining Basin, NE Tibetan Plateau, and its constraints on paleontological, sedimentological and tectonomorphological evolution, *Earth-Sci. Rev.*, *190*, 460-485. Doi: 10.1016/j.earscirev.2019.01.021.

Gilder, S., Y. Chen, and S. Sen (2001), Oligo-Miocene magnetostratigraphy and rock magnetism of the Xishuigou section, Subei (Gansu Province, western China) and implications for shallow inclinations in central Asia, *J. Geophys. Res.*, *106*(12), 30505-30522. Doi: 10.1029/2001JB000325.

Gong, Z., van Hinsbergen, D.J.J., Vissers, R.L.M., Dekkers, M.J (2009), Early Cretaceous syn-rotational extension in the Organyà basin—New constraints on the palinspastic position of Iberia during its rotation, *Tectonophysics*, *473,* 312-323. Doi: 10.1016/j.tecto.2009.03.003.

Guo, Z., W. F. Ruddiman, Q. Hao, H. Wu, Y. Qiao, R. X. Zhu, S. Peng, J. Wei, B. Yuan, and T. Liu (2002), Onset of Asian desertification by 22 Myr ago inferred from loess deposits in China, *Nature*, *416*(6877), 159-163, Doi: 10.1038/416159a.

Hetzel, R., I. Dunkl, V. Haider, M. Strobl, H. von Eynatten, L. Ding, and D. Frei (2011), Peneplain formation in southern Tibet predates the India-Asia collision and plateau uplift, *Geology*, *39*(10), 983-986. Doi:10.1130/G32069.

Hu, X., E. Garzanti, T. Moore, and I. Raffi (2015), Direct stratigraphic dating of India-Asia collision onset at the Selandian (middle Paleocene, 59 ± 1 Ma), *Geology*, *43*(10), 859-862. Doi: 10.1130/g36872.1.

Huang, B., J. Piper, S. Peng, T. Liu, Z. Li, Q. Wang, and R. Zhu (2006), Magnetostratigraphic study of the Kuche Depression, Tarim Basin, and Cenozoic uplift of the Tian Shan Range, Western China, *Earth Planet. Sci. Lett.*, *251*(3-4), 346-364. Doi: 10.1016/j.epsl.2006.09.020.

Ji, J., K. Zhang, P. D. Clift, G. Zhuang, B. Song, X. Ke, and Y. Xu (2017), High-resolution magnetostratigraphic study of the Paleogene-Neogene strata in the Northern Qaidam Basin: Implications for the growth of the Northeastern Tibetan Plateau, *Gond. Res.*, *46*, 141-155. Doi: 10.1016/j.gr.2017.02.015.

Jian, X., P. Guan, W. Zhang, H. Liang, F. Feng, and L. Fu (2018), Late Cretaceous to early Eocene deformation in the northern Tibetan Plateau: Detrital apatite fission track evidence from northern Qaidam basin, *Gond. Res.*, *60*, 94-104. Doi: 10.1016/j.gr.2018.04.007.

Jin, C., et al. (2018), Magnetostratigraphy of the Fenghuoshan Group in the Hoh Xil Basin and its tectonic implications for India–Eurasia collision and Tibetan Plateau deformation, *Earth Planet. Sci. Lett.*, *486*, 41-53. Doi: 10.1016/j.epsl.2018.01.010.

Jolivet, M., M. Brunel, D. Seward, Z. Xu, J. Yang, F. Roger, P. Tapponnier, J. Malavieille, N. Arnaud, and C. Wu (2001), Mesozoic and Cenozoic tectonics of the northern edge of the Tibetan plateau: fission-track constraints, *Tectonophysics*, *343*(1-2), 111-134. Doi: 10.1016/S0040-1951(01)00196-2.

Kapp, P., and P. DeCelles (2019), Mesozoic-Cenozoic geological evolution the Himalayan-Tibetan orogen and working tectonic hypothese *Am. J. Sci.*, *319, 159-254*. Doi: 10.2475/03.2019.01.

Kodama, K. P. (1997), A successful rock magnetic technique for correcting paleomagnetic inclination shallowing: Case study of the Nacimiento Formation, New Mexico, *J. Geophys. Res.*, *102*(B3), 5193-5205. Doi: 10.1029/96JB03833.

Kruiver, P., M. J. Dekkers, and D. Heslop (2001), Quantification of magnetic coercivity components by the analysis of acquisition curves of isothermal remanent magnetisation, *Earth Planet. Sci. Lett.*, *189*(3), 269-276. Doi: 10.1016/S0012-821X(01)00367-3.

Larrasoana, J., E. L. Pueyo, and J. M. Paré¦s (Eds.) (2004), *An integrated AMS, structural, palaeo-and rock-magnetic study of Eocene marine marls from the Jaca-Pamplona basin (Pyrenees, N Spain); new insights into the timing of magnetic fabric acquisition in weakly deformed mudrocks*, 127-143 pp., Geological Society, London, Special Publications, London. Doi:10.1144/GSL.SP.2004.238.01.10.

Li, S. H., E. L. Advokaat, D. J. J. van Hinsbergen, M. Koymans, C. Deng, and R. Zhu (2017), Paleomagnetic constraints on the Mesozoic-Cenozoic paleolatitudinal and rotational history of Indochina and South China: Review and updated kinematic reconstruction, *Earth-Sci. Rev.*, *171*, 58-77. Doi: 10.1016/j.earscirev.2017.05.007.

Li, S. H., C. L. Deng, P. Greig, H. T. Yao, S. Huang, C. Y. Liu, H. Y. He, Y. X. Pan, and R. X. Zhu (2014), Tectonic and sedimentary evolution of the late Miocene–Pleistocene Dali Basin in the southeast margin of the Tibetan Plateau: Evidences from anisotropy of magnetic susceptibility and rock magnetic data, *Tectonophysics*, *629*(0), 362-377. Doi: 10.1016/j.tecto.2014.05.035.

Li, S., van Hinsbergen, D.J.J., Najman, Y., Jing, L-Z., Deng, C., and Zhu, R (2020), Does pulsed Tibetan deformation correlate with Indian plate motion changes?, *Earth Planet. Sci. Lett.*, In press.

Maffione, M., C. Hernandez-Moreno, M. C. Ghiglione, F. Speranza, D. J. J. van Hinsbergen, and E. Lodolo (2015), Constraints on deformation of the Southern Andes since the Cretaceous from anisotropy of magnetic susceptibility, *Tectonophysics*, *665*, 236-250. Doi: 10.1016/j.tecto.2015.10.008.

Mattei, M., L. Sagnotti, C. Faccenna, and R. Funiciello (1997), Magnetic fabric of weakly deformed clay-rich sediments in the Italian peninsula: Relationship with compressional and extensional tectonics, *Tectonophysics*, *271*(1), 107-122. Doi: 10.1016/S0040-1951(96)00244-2.

Molnar, P. (2004), Late cenozoic increase in accumulation rates of terrestrial sediment: How might climate change have affected erosion rates?, *Annu. Rev. Earth Planet. Sci. Lett.*, *32*, 67-89. Doi: 10.1146/annurev.earth.32.091003.143456.

Molnar, P., and J. M. Stock (2009), Slowing of India's convergence with Eurasia since 20 Ma and its implications for Tibetan mantle dynamics, *Tectonics*, *28*(3), Doi: 10.1029/2008tc002271.

Oncken, O., Hindle, D., Kley, J., Elger, K., Victor, P., Schemmann, K (2006), Deformation of the central Andean upper crustal system—Facts, fiction, and constraints for plateau models, The Andes. Springer, pp. 3-27.

Parés, J. (Ed.) (2004), *How deformed are weakly deformed mudrocks? Insights from magnetic anisotropy, in: F Martín-Hernández, C. M.Lüneburg, C. Aubourg, M.*

Jackson(Eds.), Magnetic Fabric: Methods and Applications, 191-203 pp., Geological Society, London, Special Publications, London. Doi: 10.1144/GSL.SP.2004.238.01.13.

Parés, J., B. A. van der Pluijm, and J. Dinarès-Turell (1999), Evolution of magnetic fabrics during incipient deformation of mudrocks (Pyrenees, northern Spain), *Tectonophysics*, *307*(1), 1-14. Doi: 10.1016/S0040-1951(99)00115-8.

Patriat, P., and J. Achache (1984), India–Eurasia collision chronology has implications for crustal shortening and driving mechanism of plates, *Nature*, *311*, 615-621. Doi: 10.1038/311615a0.

Rowley, D. B. (1996), Age of initiation of collision between India and Asia: A review of stratigraphic data, *Earth Planet. Sci. Lett.*, *145*(1-4), 1-13. Doi: 10.1016/S0012-821X(96)00201-4.

Sagnotti, L., F. Speranza, A. Winkler, M. Mattei, and R. Funiciello (1998), Magnetic fabric of clay sediments from the external northern Apennines (Italy), *Phys. Earth Planet In.*, *105*(1), 73-93. Doi: 10.1016/S0031-9201(97)00071-X.

Soto, R., J. C. Larrasoaña, L. E. Arlegui, E. Beamud, B. Oliva-Urcia, and J. L. Simón (2009), Reliability of magnetic fabric of weakly deformed mudrocks as a palaeostress indicator in compressive settings, *J. Struct. Geol.*, *31*(5), 512-522. Doi:10.1016/j.jsg.2009.03.006.

Staisch, L. M., N. A. Niemi, C. Hong, M. K. Clark, D. B. Rowley, and B. Currie (2014), A Cretaceous-Eocene depositional age for the Fenghuoshan Group, Hoh Xil Basin: Implications for the tectonic evolution of the northern Tibet Plateau, *Tectonics*. 33, Doi: 10.1002/2013TC003367.

Studnicki-Gizbert, C., B. C. Burchfiel, Z. Li, and Z. Chen (2008), Early Tertiary Gonjo basin, eastern Tibet: Sedimentary and structural record of the early history of India-Asia collision, *Geos.*, *4*(4), 713-735. Doi: 10.1130/GES00136.1.

Tang, M., J. Liu-Zeng, G. D. Hoke, Q. Xu, W. Wang, Z. Li, J. Zhang, and W. Wang (2017), Paleoelevation reconstruction of the Paleocene-Eocene Gonjo basin, SE-central Tibet, *Tectonophysics*, *712-713*, 170-181. Doi: 10.1016/j.tecto.2017.05.018.

Tang, Z., B. Huang, X. Dong, J. Ji, and Z. Ding (2012), Anisotropy of magnetic susceptibility of the Jingou River section: Implications for late Cenozoic uplift of the Tian Shan, *Geochem Geophy Geosy*, *13*. Doi: 10.1029/2011GC003966.

Tarling, D., and F. Hrouda (1993), *The magnetic anisotropy of rocks*, Champan and Hall, London, 217 pp.

Tauxe, L. (2010), *Essentials of Paleomagnetism*, University of California Press, Berkeley, 512 pp.

van Hinsbergen, D. J. J., B. Steinberger, P. V. Doubrovine, and R. Gassmöller (2011), Acceleration and deceleration of India-Asia convergence since the Cretaceous: Roles of mantle plumes and continental collision, *J. Geophys. Res.*, *116*(B06101). Doi: 10.1029/2010jb008051.

van Hinsbergen, D. J., P. C. Lippert, G. Dupont-Nivet, N. McQuarrie, P. V. Doubrovine, W. Spakman, and T. H. Torsvik (2012), Greater India Basin hypothesis and a two-stage Cenozoic collision between India and Asia, *Proc. Natl. Acad. Sci. USA*, *109*(20), 7659-7664. Doi: 10.1073/pnas.1117262109.

van Hinsbergen, D. J. J., P. C. Lippert, S. Li, W. Huang, E. L. Advokaat, and W. Spakman (2019), Reconstructing Greater India: Paleogeographic, kinematic, and geodynamic perspectives, *Tectonophysics*, *760*, 69-94. Doi: 10.1016/j.tecto.2018.04.006.

van Hinsbergen, D.J.J., Torsvik, T., Schmid, S.M., Matenco, L., Maffione, M., Vissers, R.L.M., Gürer, D., Spakman, W. (2020), Orogenic architecture of the Mediterranean region and kinematic reconstruction of its tectonic evolution since the Triassic. *Gond. Res., 81*, 79-229. Doi: 10.1016/j.gr.2019.07.009.

Xizang BGMR. (1993), *Regional geology of Xizang (Tibet) Autonomous Region, Geological Memoirs Series*, Geological House, Beijing.

Yin, A., et al. (2002), Tectonic history of the Altyn Tagh fault system in northern Tibet inferred from Cenozoic sedimentation, *Geol. Soc. Am. Bull.*, *114*(10), 1257-1295. Doi: 10.1130/0016-7606(2002)114<1257:THOTAT>2.0.CO;2.

Yue, L. P., F. Heller, Z. X. Qiu, L. Zhang, G. P. Xie, Z. D. Qiu, and Y. X. Zhang (2001), Magnetostratigraphy and pavleo-environmental record of Tertiary deposits of Lanzhou Basin, *Chinese Sci. Bull.*, *46*(1), 770-773. Doi: 10.1007/BF03187220.

Zhu, D. C., Q. Wang, Z. D. Zhao, S. L. Chung, P. A. Cawood, Y. Niu, S. A. Liu, F. Y. Wu, and X. X. Mo (2015), Magmatic record of India-Asia collision, *Sci. Rep.*, *5*, 14289. Doi: 10.1038/srep14289.

Zhu, R., Q. Liu, and M. J. Jackson (2004), Paleoenvironmental significance of the magnetic fabrics in Chinese loess-paleosols since the last interglacial (< 130 ka), *Earth Planet. Sci. Lett.*, *221*(1), 55-69. Doi: 10.1016/S0012-821X(04)00103-7.

Figure Captions

Figure 1. (a) Simplified tectonic map of the Tibetan Plateau showing the distribution of main sutures (red dashed lines), sedimentary basins (orange) and related strike-slip and thrust faults (black solid lines). The blue polygon denotes the location of the Gonjo Basin in Fig. 1b. Main abbreviations: HXB: Hoh Xil Basin; NYB: Nangqian-Yushu Basin; GJB: Gonjo Basin; XNB: Xining Basin; LZB: Lanzhou Basin; YLF: Yangla thrust fault; EHS: Eastern Himalaya Syntaxis. (b) Geological map of the Gonjo Basin and surrounding area. (c) cross-section showing the asymmetric syncline of the Gonjo Basin along the Gonjo city A-A´, modified from Studnicki-Gizbert et al. (2008). (d) The overall AMS results from the Gonjo Basin, incuding the equal-area projections of AMS principal axes in geographic and stratigraphic coordinate, P_J-Km, and P_J-T diagrams.

Figure 2. (a) Lithology, (b) mean susceptibility (Km), (c) corrected degree of anisotropy (P_J) (note the different scale before and after 765 m), (d) shape parameter (T), (e) inclinations of minimum principle axes (K3_Inc), (f) declinations of maximum principle axes (K1_Dec), (g) paleomagnetic declinations, and (h) sedimentation rate from the Gonjo Basin against

thickness. (i, j) magnetostratigraphic result of the Gonjo Basin (Li et al., 2020). CW: clockwise, CCW: counter-clockwise. The red lines in b-e are seven points average smooth. The orange lines in f-g show the synchronous rotation patterns between paleomagnetic declinations and AMS K_1 declinations. The AMS parameter can be subdivided into three intervals as shown by the grey lines (see text for detail). The dashed line represents the onset of India-Asia collision at 59±1 Ma. Note that both AMS parameters, sedimentation rate, and paleomagnetic declinations do not show any change at the time of India-Asia initial collision.

Figure 3. Equal-area projections of the three principle axes, P_J-Km, and P_J–T of the three intervals as shown in Fig. 2. (a) Interval I (0-765 m, 69-65.4 Ma), (b) Interval II (765-2154.5 m, 65.4-52 Ma), and (c) Interval III (2154.5-3325 m, 52-41.5 Ma). The grey line with arrow represents the synopsis P_J-T path with increasing deformation intensity (Parés et al., 2004).

Figure 4. The isothermal remanent magnetization (IRM) acquisition curves (left) and their corresponding component analyses (right) on representative samples from the Gonjo Basin. 1 and 2 represent the low- and high-coercivity component, respectively, with $B_{1/2}$ and relative contributions to saturation IRM afterward.

Figure 1.

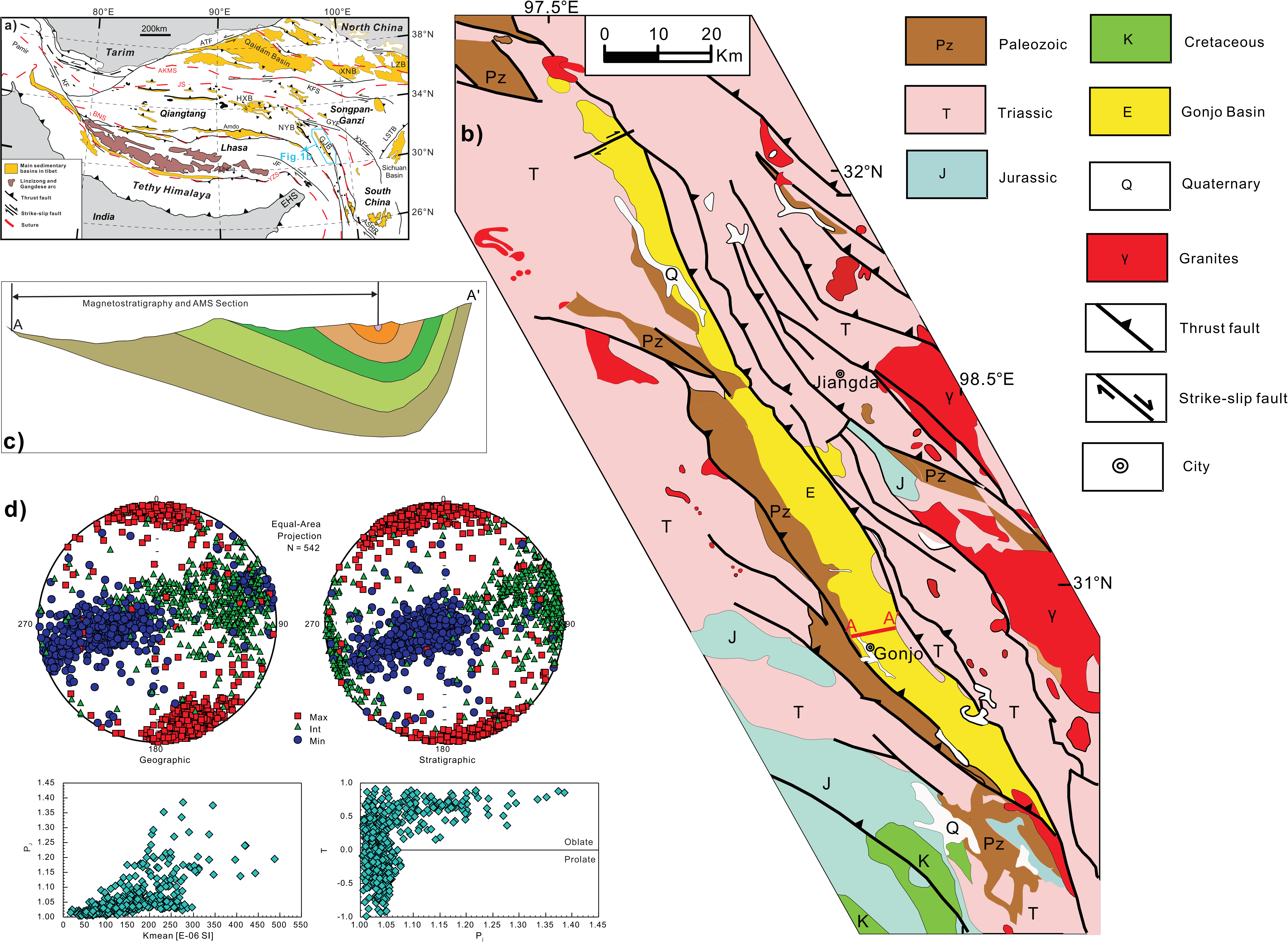

a)
b)
c)
d)
80°E
90°E
100°E
38°N
34°N
30°N
26°N
200km
North China
Tarim
Qaidam Basin
Qiangtang
Songpan-Ganzi
Lhasa
Tethy Himalaya
India
South China
Sichuan Basin
Fig.1b
Main sedimentary basins in tibet
Linzizong and Gangdese arc
Thrust fault
Strike-slip fault
Suture
97.5°E
98.5°E
32°N
31°N
0
10
20
Km
Jiangda
Gonjo
Pz
Paleozoic
T
Triassic
J
Jurassic
K
Cretaceous
E
Gonjo Basin
Q
Quaternary
γ
Granites
Thrust fault
Strike-slip fault
City
Magnetostratigraphy and AMS Section
A
A'
Equal-Area Projection
N = 542
Max
Int
Min
Geographic
Stratigraphic
Kmean [E-06 SI]
Oblate
Prolate

Figure 2.

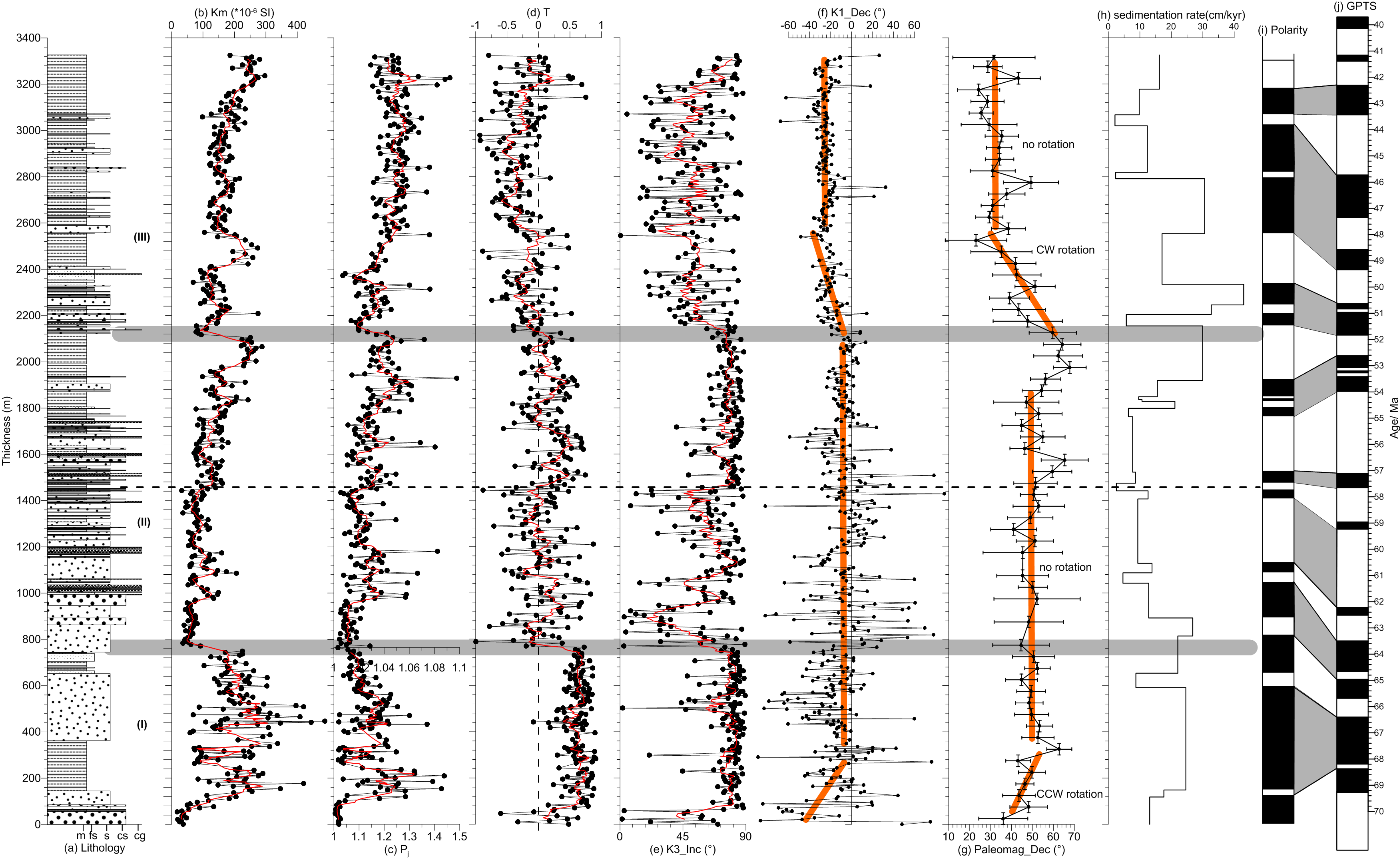

(a) Lithology
(b) Km (*10-6 SI)
(c) Pj
(d) T
(e) K3_Inc (°)
(f) K1_Dec (°)
(g) Paleomag_Dec (°)
(h) sedimentation rate(cm/kyr)
(i) Polarity
(j) GPTS
Thickness (m)
Age/ Ma
m fs s cs cg
(I)
(II)
(III)
no rotation
CW rotation
no rotation
CCW rotation

Figure 3.

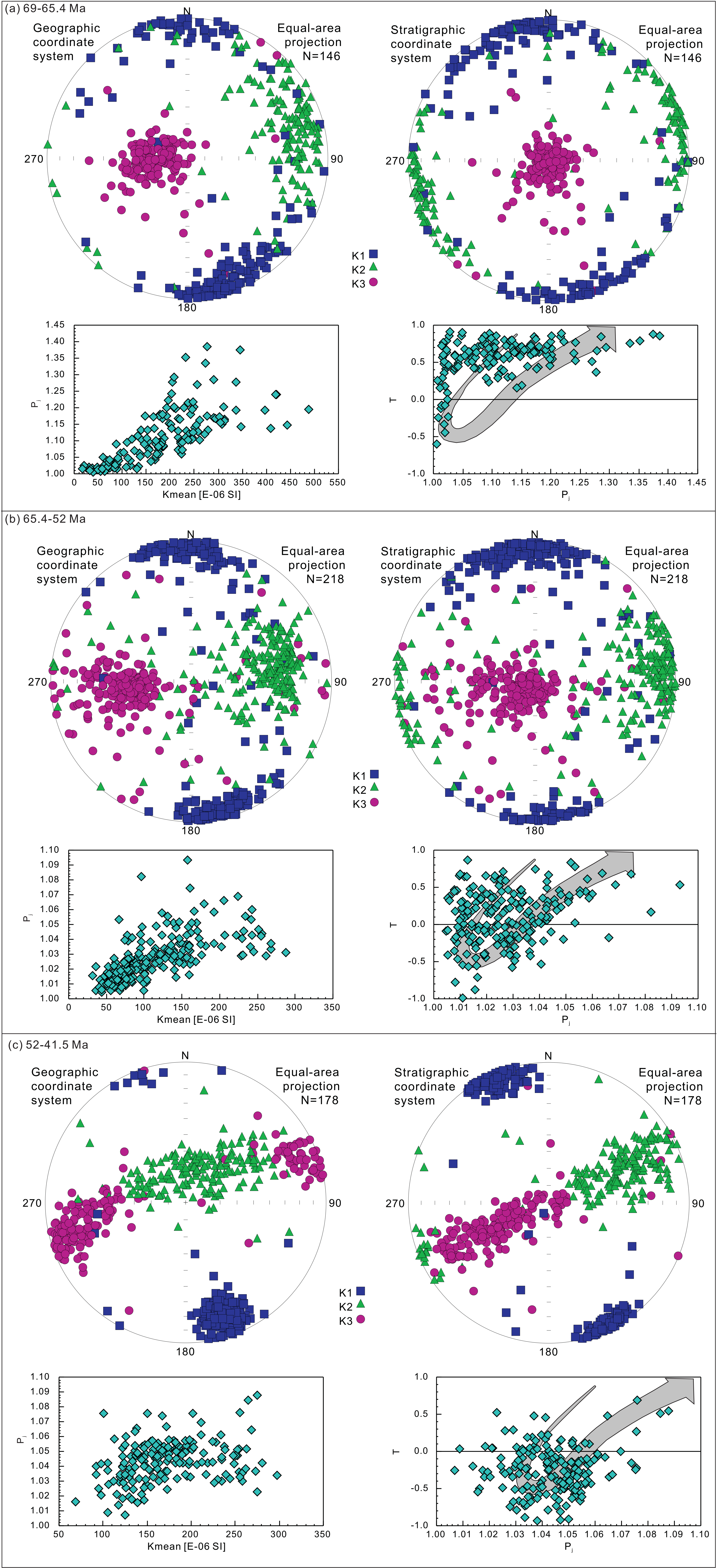

(a) 69-65.4 Ma
Geographic coordinate system
Stratigraphic coordinate system
Equal-area projection N=146
N
90
180
270
K1
K2
K3
Pj
Kmean [E-06 SI]
T
Pj
(b) 65.4-52 Ma
Geographic coordinate system
Stratigraphic coordinate system
Equal-area projection N=218
K1
K2
K3
Pj
Kmean [E-06 SI]
T
Pj
(c) 52-41.5 Ma
Geographic coordinate system
Stratigraphic coordinate system
Equal-area projection N=178
K1
K2
K3
Pj
Kmean [E-06 SI]
T
Pj

Figure 4.

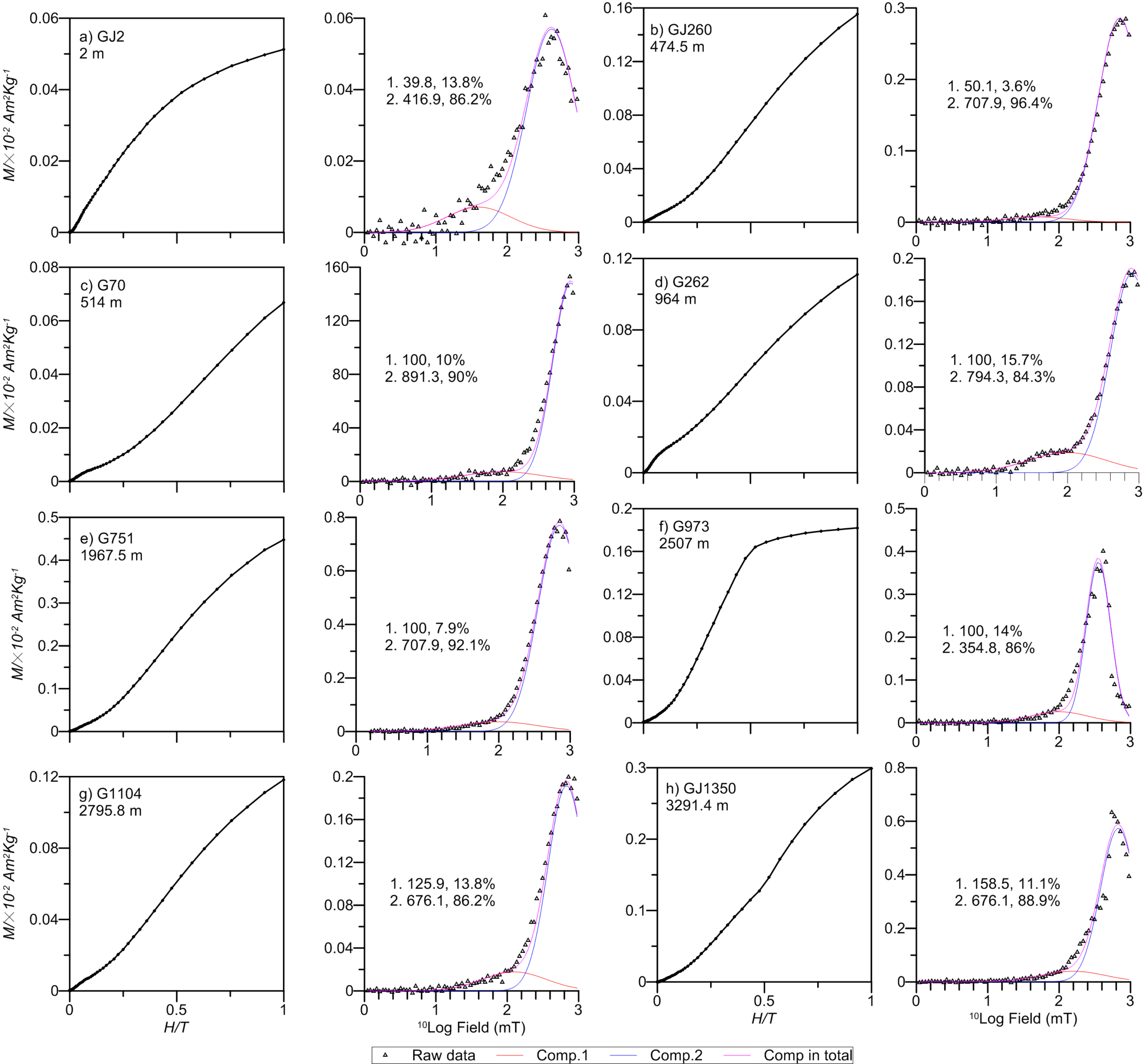

a) GJ2
2 m
1. 39.8, 13.8%
2. 416.9, 86.2%
b) GJ260
474.5 m
1. 50.1, 3.6%
2. 707.9, 96.4%
c) G70
514 m
1. 100, 10%
2. 891.3, 90%
d) G262
964 m
1. 100, 15.7%
2. 794.3, 84.3%
e) G751
1967.5 m
1. 100, 7.9%
2. 707.9, 92.1%
f) G973
2507 m
1. 100, 14%
2. 354.8, 86%
g) G1104
2795.8 m
1. 125.9, 13.8%
2. 676.1, 86.2%
h) GJ1350
3291.4 m
1. 158.5, 11.1%
2. 676.1, 88.9%
M/×10^-2 Am^2Kg^-1
H/T
^10Log Field (mT)
Raw data
Comp.1
Comp.2
Comp in total